



1 **Estimation of the fossil-fuel component in atmospheric CO₂ based on**
2 **radiocarbon measurements at the Beromünster tall tower, Switzerland**

3

4 Tesfaye A. Berhanu¹, Sönke Szidat², Dominik Brunner³, Ece Satar¹, Rüdiger Schanda¹, Peter
5 Nyfeler¹, Michael Battaglia², Martin Steinbacher³, Samuel Hammer⁴ and Markus
6 Leuenberger¹

7 ¹*Climate and Environmental Physics, Physics Institute and Oeschger Centre for Climate Change Research,*
8 *University of Bern, Bern, Switzerland*

9 ²*Department of Chemistry and Biochemistry and Oeschger Center for Climate Change Research, University of*
10 *Bern, Bern, Switzerland*

11 ³*Empa, Laboratory for Air Pollution/Environmental Technology, Dübendorf, Switzerland*

12 ⁴*Institut für Umweltp Physik, Universität Heidelberg, Heidelberg, Germany*

13 Abstract

14 Fossil fuel CO₂ (CO_{2ff}) is the major contributor of anthropogenic CO₂ in the atmosphere, and
15 accurate quantification is essential to better understand the carbon cycle. Since October 2012,
16 we have been continuously measuring the mixing ratios of CO, CO₂ CH₄ and H₂O at five
17 different heights at the Beromünster tall tower, Switzerland. Air samples for radiocarbon
18 ($\Delta^{14}\text{CO}_2$) analysis have also been collected from the 212.5 m sampling inlet of the tower on a
19 bi-weekly basis. A correction was applied for ¹⁴CO₂ emissions from nearby nuclear power
20 plants (NPPs), which have been simulated with the Lagrangian transport model FLEXPART-
21 COSMO. The ¹⁴CO₂ emissions from NPPs offset the depletion in ¹⁴C by fossil-fuel emissions
22 resulting in an underestimation of the fossil-fuel component in atmospheric CO₂ by about 16
23 %. An average observed ratio (R_{CO}) of 13.4 ± 1.3 mmol/mol was calculated from the
24 enhancements in CO mixing ratios relative to the clean air reference site Jungfrauoch (ΔCO)
25 and the radiocarbon-based fossil-fuel CO₂ mole fractions. This ratio is significantly higher



26 than both the mean anthropogenic CO/CO₂ emission ratios estimated for Switzerland from the
27 national inventory (7.8 mmol/mol for 2013), and the ratio between in-situ measured CO and
28 CO₂ enhancements at Beromünster over the Jungfrauoch background (8.3 mmol/mol).
29 Differences could not yet be assigned to specific processes and shortcomings of these two
30 methods but may originate from locally variable emission ratios as well as from non-fossil
31 emissions and biospheric contributions. By combining the ratio derived using the radiocarbon
32 measurements and the in-situ measured CO mixing ratios, a high-resolution time series of
33 CO_{2ff} was calculated exhibiting a clear seasonality driven by seasonal variability in emissions
34 and vertical mixing. By subtracting the fossil-fuel component and the large-scale background,
35 we have determined the regional biospheric CO₂ component that is characterized by seasonal
36 variations ranging between -15 to +30 ppm. A pronounced diurnal variation was observed
37 during summer modulated by biospheric exchange and vertical mixing while no consistent
38 pattern was found during winter.

39 **1. Introduction**

40 Fossil fuel CO₂ (CO_{2ff}) is the fundamental contributor to the increase in atmospheric
41 CO₂, hence its precise quantification is crucial to better understand the global carbon budget.
42 One of the major uncertainties in the projections of climate change is the uncertainty in the
43 future carbon budget due to feedbacks between terrestrial ecosystems and climate (Heimann
44 and Reichstein, 2008). Information on the response of the biosphere to climate variations can
45 be obtained from atmospheric CO₂ observations, but isolating the biospheric signal in the
46 measured CO₂ mixing ratios requires an accurate quantification of the fossil fuel component.
47 Several methods have therefore been proposed for quantifying CO_{2ff}, which are based on
48 observations or models. A widely employed approach is to determine CO_{2ff} with an
49 atmospheric transport model that incorporates CO_{2ff} emissions from a bottom-up emission
50 inventory.



51 Emission inventories are based on statistics of the energy-use by different sectors and
52 the quantification of CO_{2ff} emissions by accounting for the carbon content of each fuel and its
53 corresponding oxidation ratios (Friedlingstein et al., 2010; Le Quéré et al., 2016). When
54 compared to other greenhouse gases, national emission inventories for CO₂ are quite accurate,
55 but the computation of these inventories is laborious, and the quality depends on the energy
56 statistics and reporting methods that vary strongly between countries (Marland, 2008;
57 Marland et al., 2009). A recent study evaluating different energy statistics and cement
58 production data estimated an uncertainty of about 5 % for the global fossil-fuel emissions of
59 the past decade (2006 – 2015)(Le Quéré et al., 2016). At country level the uncertainties are
60 usually below 5 % in developed countries but often exceed 10 % in developing countries
61 (Ballantyne et al., 2015).

62 Additional uncertainties arise from the spatial and temporal disaggregation of national
63 annual total emissions to the grid of the atmospheric transport model. At sub-country scales
64 (less than 150 km), the uncertainty from bottom-up estimates can reach up to 50 % (Ciais et
65 al., 2010). Finally, errors in the transport model and the inability to correctly represent point
66 observations in the model may contribute substantially to the uncertainty of model simulated
67 CO_{2ff} mixing ratios (Tolk et al., 2008; Peylin et al., 2011).

68 Radiocarbon measurements can be used to directly quantify CO_{2ff} in atmospheric CO₂
69 observations. Radiocarbon is produced in the lower stratosphere during the reaction of
70 neutrons with nitrogen induced by cosmic rays (Currie, 2004). In addition, nuclear bomb tests
71 in the 1960s led to large radiocarbon input into the atmosphere which was thereafter
72 decreasing due to gradual uptake by the oceans and the terrestrial biosphere. Nowadays, the
73 decline in atmospheric ¹⁴C is mainly driven by input from ¹⁴C-free fossil fuel CO₂ (Levin et
74 al., 2010). This decline is well detectable at background sites such as Jungfraujoeh,
75 Switzerland and Schauinsland, Germany (Levin et al., 2013). While all reservoirs exchanging



76 carbon with the atmosphere are relatively rich in ^{14}C , fossil-fuels (millions of years old) are
77 devoid of ^{14}C due to its radioactive decay with a half-life of 5370 years. Hence, any fossil-fuel
78 CO_2 emitted to the atmosphere will dilute the background ^{14}C signal, the so-called Suess
79 effect, which can then be used to unravel recently added fossil-fuel CO_2 to the atmosphere
80 (Zondervan and Meijer, 1996; Levin et al., 2003; Gamnitzer et al., 2006; Turnbull et al., 2006;
81 Levin and Karstens, 2007; Turnbull et al., 2009; Turnbull et al., 2011; Lopez et al., 2013;
82 Turnbull et al., 2014; Turnbull et al., 2015). However, this depletion can also partially be
83 offset by CO_2 release from the biosphere which has enriched $^{14}\text{C}/^{12}\text{C}$ ratios due to the bomb
84 tests as well as by direct ^{14}C emissions from the nuclear industries (Levin et al 2010). This
85 technique also enables to separate between biospheric and fossil-fuel CO_2 components in
86 atmospheric CO_2 observations, and thus to better constrain the biospheric CO_2 fluxes when
87 coupled with inversion models (Basu et al., 2016). The uncertainty in $\text{CO}_{2\text{ff}}$ estimated by the
88 radiocarbon method is mainly determined by the precision in the ^{14}C measurement, the choice
89 of background as well as the contribution from other sources of ^{14}C such as nuclear power
90 plants (NPPs) (Turnbull et al., 2009).

91 Despite its importance as a fossil-fuel tracer, measurements of ^{14}C are still sparse. The
92 measurements are expensive and laborious, which so far has prevented frequent sampling and
93 has motivated researchers to combine ^{14}C measurements with additional tracers such as CO to
94 enhance spatial and temporal coverage (Gamnitzer et al., 2006; Levin and Karstens, 2007;
95 Vogel et al., 2010; Lopez et al., 2013; Turnbull et al., 2014; Turnbull et al., 2015). The CO-
96 method relies on using high frequency CO measurements and regular calibration of the
97 temporally changing $\Delta\text{CO}:\Delta\text{CO}_{2\text{ff}}$ ratios based on weekly or bi-weekly ^{14}C measurements.
98 Despite its advantage of providing a proxy for continuous $\text{CO}_{2\text{ff}}$ data, the method introduces
99 additional uncertainties due to diurnal and seasonal variability in the CO sink, and the
100 presence of multiple non-fossil CO sources such as oxidation of hydrocarbons or wood and



101 biofuel combustion (Gamnitzer et al., 2006). Spatial variations in the $\Delta\text{CO}:\Delta\text{CO}_2$ ratio across
102 Europe due to different source compositions and environmental regulations, which affects the
103 measured ratios due to changes in air mass origin (Oney et al., In review) are the main reason
104 for the temporally changing $\Delta\text{CO}:\Delta\text{CO}_{2\text{ff}}$ ratio for a given measurement site.

105 In Switzerland, CO_2 contributes about 82 % of the total greenhouse gas emissions
106 according to the Swiss national emission inventory for 2013, and fossil-fuel combustion from
107 the energy sector contributes more than 80 % of the total CO_2 emission (FOEN, 2015b). In
108 order to validate such bottom-up estimates, independent techniques based on atmospheric
109 measurements are desirable. In addition, as mentioned above, the biospheric CO_2 signals can
110 only be estimated with a good knowledge of $\text{CO}_{2\text{ff}}$. In this study, we present and discuss
111 $^{14}\text{CO}_2$ measurements conducted bi-weekly between 2013 and 2015 at the Beromünster tall
112 tower in Switzerland. From these samples in combination with background CO , CO_2 and
113 $^{14}\text{CO}_2$ measurements at the high-altitude remote location Jungfrauoch, Switzerland, ΔCO to
114 $\Delta\text{CO}_{2\text{ff}}$ ratios (R_{CO}) are derived. These ratios are then combined with the in-situ measured
115 ΔCO mixing ratios to estimate a high-resolution time series of atmospheric $\text{CO}_{2\text{ff}}$ mixing
116 ratios, and by difference, of the biospheric CO_2 component. The influence of ^{14}C emissions
117 from nearby NPPs and correction strategies are also discussed.

118 2. Methods

119 2.1. Site description and continuous measurement of CO and CO_2

120 A detailed description of the Beromünster tall tower measurement system as well as a
121 characterization of the site with respect to local meteorological conditions, seasonal and
122 diurnal variations of greenhouse gases, and regional representativeness can be obtained from
123 previous publications (Oney et al., 2015; Berhanu et al., 2016; Satar et al., 2016). In brief, the
124 tower is located near the southern border of the Swiss Plateau, the comparatively flat part of
125 Switzerland between the Alps in the south and the Jura mountains in the northwest ($47^\circ 11'$



126 23° N, 8° 10' 32" E, 797 m a.s.l.), which is characterized by intense agriculture and rather
127 high population density (Fig. 1). The tower is 217.5 m tall with access to five sampling
128 heights (12.5 m, 44.6 m, 71.5 m, 131.6 m, 212.5 m) for measuring CO, CO₂, CH₄ and H₂O
129 using Cavity Ring Down Spectroscopy (CRDS) (Picarro Inc., G-2401). By sequentially
130 switching from the highest to the lowest level, mixing ratios of these trace gases were
131 recorded continuously for three minutes per height, but only the last 60 seconds were retained
132 for data analysis. The calibration procedure for ambient air includes measurements of
133 reference gases with high and low mixing ratios traceable to international standards (WMO-
134 X2007 for CO₂ and WMO-X2004 for CO and CH₄), as well as target gas and more frequent
135 working gas determinations to ensure the quality of the measurement system. From two years
136 of data a long-term reproducibility of 2.79 ppb, 0.05 ppm, and 0.29 ppb for CO, CO₂ and
137 CH₄, respectively was determined for this system (Berhanu et al., 2016).

138 2.2. Sampling and CO₂ extraction for isotope analysis

139 Air samples for ¹⁴C₂O analysis were collected every second week from the highest
140 inlet usually between 9:00 to 13:00 UTC. During each sampling event, three samples were
141 collected over a 15-minute interval in 100 L PE-AL-PE bags (TESSERAUX, Germany) from
142 the flush pump exhaust line of the 212.5 m sampling inlet, which has a flow rate of about 9 L
143 min⁻¹ at ambient conditions. The sampling interval was chosen to ensure radiocarbon sample
144 collection in parallel with the continuous CO and CO₂ measurements by the CRDS analyzer
145 at the highest level. Each bag was filled at ambient air pressure for 6 to 8 minutes and a total
146 air volume of 50 to 70 L (at STP) was collected.

147 CO₂ extraction was conducted cryogenically in the laboratory at the University of
148 Bern usually the day after the sample collection. During the extraction step, the air sample
149 was first pumped through a stainless steel water trap (-75 °C), which was filled with glass
150 beads (Rashig rings, 5 mm, Germany). A flow controller (Analyt-MTC, Aalborg, USA) with



151 flow totalizer tool was attached to this trap to maintain a constant flow of air (1.2 L min^{-1})
152 towards the second trap (trap 2), a spiral-shaped stainless steel tube ($1/4''$) filled with glass
153 beads ($\sim 2 \text{ mm}$) and immersed in liquid nitrogen to freeze out CO_2 . When the flow ceased,
154 trap 2 was isolated from the line and evacuated to remove gases which are non-condensable at
155 this temperature. Then, trap 2 was warmed to room temperature, and eventually immersed in
156 slush at $-75 \text{ }^\circ\text{C}$ to freeze out any remaining water. Finally, the extracted CO_2 was expanded
157 and collected in a 50 mL glass flask immersed in liquid nitrogen.

158 Sample extraction efficiency was calculated by comparing the amount of the
159 cryogenically extracted CO_2 with the CO_2 measured in-situ by the CRDS analyzer during the
160 time of sampling. The amount of CO_2 extracted is determined first by transferring the
161 extracted CO_2 cryogenically to a vacuum line of predetermined volume. Then, based on the
162 pressure reading of the expanded gas, and the total volume of air collected determined by the
163 mass flow controller with a totalizer function attached to trap 1, CO_2 mixing ratios were
164 calculated.

165 At the end of 2014 we noticed that there was a leakage from the sampling line exhaust
166 pumps, which resulted in unrealistically high CO_2 mixing ratios (usually more than 500 ppm).
167 Therefore, we replaced all the exhaust pumps and the leakage problem was solved. Seven
168 samples, which were suspected to be contaminated due to this issue, were consequently
169 excluded. The sample extraction efficiency since then has usually been better than 99 %. We
170 also made a blank test to check the presence of any leaks or contamination during sample
171 processing but did not observe any of these issues.

172 2.3. Measurement of $\delta^{13}\text{C}$, $\delta^{18}\text{O}$ and $\Delta^{14}\text{C}$

173 Prior to radiocarbon measurement, the extracted CO_2 was analyzed for the stable
174 isotopes $\delta^{13}\text{C}$ and $\delta^{18}\text{O}$ using the Isotope Ratio Mass Spectrometer (Finnigan MAT 250) at the
175 Climate and Environmental Physics Division of University of Bern, which has an accuracy



176 and precision of better than 0.1 ‰ for both $\delta^{13}\text{C}$ and $\delta^{18}\text{O}$ (Leuenberger et al., 2003). ^{14}C
177 analysis of the extracted CO_2 was performed with an accelerator mass spectrometer (AMS)
178 MICADAS (MIni CARbon DAting System) at the Laboratory for the Analysis of Radiocarbon
179 (LARA) at the Department of Chemistry and Biochemistry of the University of Bern (Szidat
180 et al., 2014). An automated graphitization equipment (AGE) was used to prepare solid target
181 gas (Nemec et al., 2010) from the extracted CO_2 stored in 50 mL glass flasks. A measurement
182 series consisted of up to 15 air samples converted to 30 solid graphite targets (duplicates),
183 together with four and three targets from CO_2 produced by combustion of the NIST standard
184 oxalic acid II (SRM 4990C) and fossil CO_2 (Carbagas, Gümliigen), respectively, which were
185 used for the blank subtraction, standard normalization, and correction for isotopic
186 fractionations. Data reduction was performed using the BATS program (Wacker et al., 2010).
187 As $^{14}\text{C}/^{12}\text{C}$ from Beromünster was measured at the LARA laboratory in Bern, whereas the
188 corresponding background samples from Jungfrauoch were analyzed at the Institute of
189 Environmental Physics, Heidelberg University, the datasets needed to be adjusted to each
190 other. A recent interlaboratory compatibility test estimated a small bias of 2.1 ± 0.5 ‰
191 (Hammer et al., 2016) between the two institutes, which was subsequently subtracted from the
192 ^{14}C measurements of the Beromünster samples.

193 2.4. Determination of the fossil fuel CO_2 component

194 2.4.1. The $\Delta^{14}\text{C}$ technique

195 For the determination of the $\text{CO}_{2\text{ff}}$ component we followed the method developed by
196 Levin and co-workers (Levin et al., 2003; Levin and Karstens, 2007). The measured CO_2 is
197 assumed to be composed of three major components: the free troposphere background
198 ($\text{CO}_{2\text{bg}}$), the regional biospheric component ($\text{CO}_{2\text{bio}}$) comprising photosynthesis and
199 respiration components, and the fossil-fuel component ($\text{CO}_{2\text{ff}}$):

$$200 \quad \text{CO}_{2\text{meas}} = \text{CO}_{2\text{bg}} + \text{CO}_{2\text{bio}} + \text{CO}_{2\text{ff}} \quad (1)$$



201 Each of these components has a specific $\Delta^{14}\text{C}$ value described as $\Delta^{14}\text{C}_{\text{meas}}$, $\Delta^{14}\text{C}_{\text{bg}}$, $\Delta^{14}\text{C}_{\text{bio}}$ and
202 $\Delta^{14}\text{C}_{\text{ff}}$. In analogy to Eq. (1), a mass balance equation can also be formulated for ^{14}C as:

$$203 \quad \text{CO}_{2\text{meas}} (\Delta^{14}\text{C}_{\text{meas}} + 1000 \text{‰}) = \text{CO}_{2\text{bg}} (\Delta^{14}\text{C}_{\text{bg}} + 1000 \text{‰}) + \text{CO}_{2\text{bio}} (\Delta^{14}\text{C}_{\text{bio}} + 1000 \\ 204 \quad \text{‰}) + \text{CO}_{2\text{ff}} (\Delta^{14}\text{C}_{\text{ff}} + 1000 \text{‰}) \quad (2)$$

205 Note that non-fossil fuel components such as biofuels are incorporated into the biospheric
206 component in Eq. (1). The fossil-fuel term in Eq. (2) is zero as fossil fuels are devoid of
207 radiocarbon ($\Delta^{14}\text{C}_{\text{ff}} = -1000 \text{‰}$). Replacing the biospheric CO_2 component in Eq. (1) by a
208 formulation derived from Eq. (2), the fossil fuel CO_2 component is derived as:

$$209 \quad \text{CO}_{2\text{ff}} = \frac{\text{CO}_{2\text{bg}} (\Delta^{14}\text{C}_{\text{bg}} - \Delta^{14}\text{C}_{\text{bio}}) - \text{CO}_{2\text{meas}} (\Delta^{14}\text{C}_{\text{meas}} - \Delta^{14}\text{C}_{\text{bio}})}{\Delta^{14}\text{C}_{\text{bio}} + 1000\text{‰}} \quad (3)$$

210 Equation (3) can be further simplified by assuming that $\Delta^{14}\text{C}_{\text{bio}}$ is equal to $\Delta^{14}\text{C}_{\text{bg}}$ (Levin et al.,
211 2003) as:

$$212 \quad \text{CO}_{2\text{ff}} = \frac{\text{CO}_{2\text{meas}} (\Delta^{14}\text{C}_{\text{bg}} - \Delta^{14}\text{C}_{\text{meas}})}{\Delta^{14}\text{C}_{\text{bg}} + 1000\text{‰}} \quad (4)$$

213 Hence, the fossil fuel CO_2 component can be determined using the $\text{CO}_{2\text{meas}}$ and $\Delta^{14}\text{C}_{\text{meas}}$
214 values measured at the site as well as $\Delta^{14}\text{C}_{\text{bg}}$ obtained from the Jungfrauoch mountain
215 background site in the Swiss Alps.

216 However, the $\text{CO}_{2\text{ff}}$ determined using Eq. (4) incorporates a small bias due to the non-
217 negligible disequilibrium contribution of heterotrophic respiration while the contribution from
218 autotrophic respiration can be approximated by $\Delta^{14}\text{C}_{\text{bg}}$. Turnbull et al. (2006) showed that this
219 effect will lead to an underestimation of $\text{CO}_{2\text{ff}}$ on average by 0.2 ppm in winter and 0.5 ppm
220 in summer, respectively, estimated for the northern hemisphere using a mean terrestrial
221 carbon residence time of 10 years. To account for this bias, a harmonic function varying
222 seasonally between these values was added to the derived $\text{CO}_{2\text{ff}}$ values. However, variation of
223 respiration fluxes on shorter timescales cannot be accounted for by this simple correction.



224 **2.4.2. Simulation of ^{14}C from nuclear power plants**

225 Radiocarbon is produced by nuclear reactions in NPPs and primarily emitted in the
226 form of $^{14}\text{CO}_2$ (Yim and Caron, 2006), except for Pressurized Water Reactors (PWR), which
227 release ^{14}C mainly in the form of $^{14}\text{CH}_4$. Previous studies have shown that such emissions can
228 lead to large-scale gradients in atmospheric $\Delta^{14}\text{C}$ activity and offset the depletion from fossil-
229 fuel emissions (Graven and Gruber, 2011). At Heidelberg in Germany, an offset of 25 % and
230 10 % of the fossil-fuel signal was observed during summer and winter, respectively, due to
231 emissions from a nearby plant (Levin et al., 2003). Similarly, Vogel et al. (2013) determined
232 the influence of NPPs for a measurement site in Canada, and estimated that about 56 % of the
233 total $\text{CO}_{2\text{ff}}$ component was masked by the contribution from NPPs. In Switzerland, there are
234 five NPPs and the closest plant is located about 30 km to the northwest of Beromünster (Fig.
235 1). Furthermore, air masses arriving at Beromünster are frequently advected from France,
236 which is the largest producer of nuclear power in Europe.

237 To estimate the influence of NPPs on $\Delta^{14}\text{C}$ at Beromünster, we used FLEXPART-
238 COSMO backward Lagrangian particle dispersion simulations (Henne et al., 2016).
239 FLEXPART-COSMO was driven by hourly operational analyses of the non-hydrostatic
240 numerical weather prediction model COSMO provided by the Swiss weather service
241 MeteoSwiss at approximately $7 \times 7 \text{ km}^2$ resolution for a domain covering large parts of
242 Western Europe. For each 3-hour measurement interval during the three-year period, a source
243 sensitivity map (footprint) was calculated by tracing the paths of 50'000 particles released
244 from Beromünster at 212 m above ground over 4 days backward in time. The source
245 sensitivities were then multiplied with the $^{14}\text{CO}_2$ emissions of all NPPs within the model
246 domain. Thereby, the emission of a given NPP was distributed over the area of the model grid
247 cell containing the NPP. Source sensitivities were calculated for three different vertical layers
248 (0-50 m, 50-200 m, 200-500 m). Since the height of ventilation chimneys of the Swiss NPPs



249 is between 99 m and 120 m, only the sensitivity of the middle layer was selected here as it
250 corresponds best to the effective release height.

251 The release of ^{14}C both in inorganic (CO_2) and organic form (CH_4) is routinely
252 measured at all Swiss NPPs. The corresponding data have been kindly provided by the Swiss
253 Federal Nuclear Safety Inspectorate (ENSI) and the Berner Kraftwerke (BKW) operating the
254 NPP Mühleberg at temporal resolutions ranging from annual (Benznau 1 & 2), to monthly
255 (Leibstadt, Gösgen), and bi-weekly (Mühleberg), and we assumed constant emissions over the
256 corresponding periods. For Beznau 1, the emissions of 2015 were distributed over the first 3
257 months of the year due to the shut-down of the plant in March 2015. The largest sources of
258 $^{14}\text{CO}_2$ in Switzerland are the two Boiling Water Reactors (BWP) Mühleberg and Leibstadt
259 (Loosli and Oeschger, 1989). Beznau 1 & 2 and Gösgen are PWRs emitting about one order
260 of magnitude less $^{14}\text{CO}_2$. For NPPs outside Switzerland, the emissions were estimated from
261 energy production data reported to the International Atomic Energy Agency (IAEA) and NPP
262 type-specific emission factors following Graven and Gruber (2011). The enhancement in $\Delta^{14}\text{C}$
263 caused by nuclear emissions at Beromünster ($\delta\Delta_{\text{nuc}}$) was then computed according to Graven
264 and Gruber (2011) as:

$$265 \quad \delta\Delta_{\text{nuc}} = \frac{\delta A_{\text{nuc}} \times 1000\text{‰}}{R_S(C_R + \delta C_{\text{ff}})} \quad (5)$$

266 where δA_{nuc} and δC_{ff} are the enhancements in $^{14}\text{CO}_2$ and CO_2 relative to a reference site with
267 a background CO_2 mixing ratio C_R , respectively. R_S represents the modern day $^{14}\text{C}/^{12}\text{C}$ ratio
268 of 1.176×10^{-12} .

269 **2.4.3. Calculation of R_{CO} , $\Delta\text{CO}/\Delta\text{CO}_2$ and high resolution $\text{CO}_{2\text{ff}}$**

270 A ΔCO to $\Delta\text{CO}_{2\text{ff}}$ ratio (R_{CO}) was calculated as the slope of the geometric mean
271 regression (model II), with ΔCO being the corresponding CO enhancement over a background
272 measured at Jungfrauoch, and the $\text{CO}_{2\text{ff}}$ values determined above. The CO measurements at



273 Jungfraujoch were conducted using a CRDS analyzer (Picarro Inc., G-2401) with a
274 measurement precision of ± 1 ppb for 10-minute aggregates (Zellweger et al., 2012).

275 As CO is usually co-emitted with CO₂ during incomplete combustion of fossil and
276 other fuels, we have also computed a tracer ratio designated as $\Delta\text{CO}/\Delta\text{CO}_2$ from the
277 enhancements in the in-situ measured CO and CO₂ mixing ratios over the Jungfraujoch
278 background (Oney et al., 2016, In review). CO_{2bg} values were obtained by applying the
279 robust extraction of baseline signal (REBS) statistical method to the continuous CO₂
280 measurements at the high altitude site Jungfraujoch (Schibig et al., 2016) with a band width of
281 60 days. Note that while R_{CO} strictly refers to the ratio of ΔCO to fossil fuel CO₂ emissions,
282 the $\Delta\text{CO}/\Delta\text{CO}_2$ ratio can be influenced by biospheric contribution as well as CO₂ emissions
283 from non-fossil sources such as biofuels and biomass burning.

284 In order to construct the high resolution CO_{2ff} time series, we combined the in-situ
285 measured CO enhancements at the Beromünster tower with the radiocarbon-derived ratios
286 R_{CO}, and estimated CO_{2ff}^{CO} for the three-year dataset as:

$$287 \quad \text{CO}_{2\text{ff}}^{\text{CO}} = \frac{\text{CO}_{\text{obs}} - \text{CO}_{\text{bg}}}{R_{\text{CO}}} \quad (6)$$

288 where CO_{obs} is the hourly averaged CO measurements at the tower. CO_{bg} is the background
289 CO values derived from measurements at the High Alpine Research Station Jungfraujoch,
290 estimated in the same way as CO_{2bg} by applying the REBS statistical method (Ruckstuhl et
291 al., 2012) with a bandwidth of 60 days to eliminate the influence of short-term local
292 variability occasionally observed at Jungfraujoch.

293 3. Results and Discussions

294 3.1. $\Delta^{14}\text{CO}_2$ and CO_{2ff}

295 Figure 2a shows the in-situ measured hourly mean CO₂ dry air mole fractions at
296 Beromünster (black) from the 212.5 m sample inlet matching at hours when air samples were



297 collected for radiocarbon analysis and the corresponding background CO₂ at Jungfraujoch
298 (blue). During the measurement period, we have recorded CO₂ mixing ratios between 389
299 ppm and 417 ppm. Spikes of CO₂ were observed mainly during winter, associated with weak
300 vertical mixing and enhanced anthropogenic emissions while lower CO₂ mixing ratios were
301 recorded during summer due to strong vertical mixing and photosynthetic uptake (Berhanu et
302 al., 2016; Satar et al., 2016).

303 Isotopic analysis of the air samples yielded $\Delta^{14}\text{C}_{\text{meas}}$ between -12.3 ‰ and +22.8 ‰,
304 with no clear seasonal trend, after correction for the model-simulated contribution from NPPs
305 (Fig. 2b). Based on the simulations described in section 2.4.2, we have calculated a mean
306 enhancement in $\Delta^{14}\text{C}$ of +1.6 ‰ and a maximum of +8.4 ‰ due to NPPs. This agrees
307 qualitatively with the coarse resolution simulations of Graven and Gruber (2011), which
308 suggest a mean enhancement of +1.4 ‰ to +2.8 ‰ over this region (Graven and Gruber,
309 2011). While about 70 % of this contribution is due to Swiss NPPs, the remaining
310 contribution is of foreign origin. About 75 % of the contribution from the Swiss NPPs is due
311 to Mühleberg, which is located west of Beromünster and hence frequently upstream of the
312 site, due to the prevailing westerly winds (Oney et al., 2015). Note that each data point
313 represents a mean value of the triplicate samples collected consecutively with a standard error
314 of 2 ‰ among triplicates. During this period, the background $\Delta^{14}\text{C}$ values measured at
315 Jungfraujoch varied between 15 ‰ and 28 ‰. Regional depletions in $\Delta^{14}\text{C}$ due to fossil-fuel
316 emissions, i.e. differences between Beromünster and the clean air reference site Jungfraujoch,
317 were in the range of -0.7 ‰ to -29.9 ‰ with a mean value of -9.9 ‰.

318 Figure 2c shows the corresponding CO_{2ff} determined after correcting for radiocarbon
319 emissions from NPPs. The typical uncertainty in CO_{2ff} is 1.1 ppm calculated from a mean
320 $\Delta^{14}\text{C}$ measurement uncertainty of 2.0 ‰ in both the sample and the background values. A
321 mean fossil-fuel CO₂ contribution of 4.3 ppm was calculated from these samples. Few cases,



322 notably the sample from 27 March 2014, showed a higher $\text{CO}_{2\text{ff}}$ and a strong depletion in
323 $\Delta^{14}\text{C}_{\text{meas}}$, consistent with the high CO_2 mixing ratio shown in the top panel. This can be due to
324 a strong local fossil-fuel contribution or a polluted air mass transported from other regions of
325 Europe coinciding with the grab samplings. As this event occurred during a period with
326 moderate temperatures (mean temperature of 6.8 °C measured at the highest level of the
327 Beromünster tower between March and May), strong fossil fuel CO_2 emissions due to heating
328 are not expected. The FLEXPART-COSMO transport simulations for this event suggest an air
329 mass origin from southeastern Europe. Periods with winds from the east, colloquially known
330 as Bise, are well known to be associated with very stable boundary layers and
331 correspondingly strong accumulation of air pollutants during the cold months of the year
332 between autumn and spring. Air masses reaching Beromünster from Eastern Europe have
333 recently been reported to contain unusually high levels of CO during late winter and early
334 spring periods, coinciding with this sampling period (Oney et al., 2016, In review).

335 By subtracting the background and fossil-fuel CO_2 contributions from the measured
336 mixing ratios, $\text{CO}_{2\text{bio}}$ values were also determined ranging between +11.2 ppm and -12.4 ppm
337 (Figure 2d). Even if there is no clear seasonal trend, the lowest $\text{CO}_{2\text{bio}}$ values were recorded
338 during summer implying net photosynthetic CO_2 uptake while most of the values in winter are
339 positive or close to zero due to respiration. Two of the samples in June and July 2015 showed
340 a rather large positive $\text{CO}_{2\text{bio}}$ contribution, in contrast to the expected summertime minimum.
341 Reasons for such high values can be biomass harvesting or enhanced respiration by plants and
342 soil, associated with warmer temperature which will lead to enhanced CO_2 emissions (Oney et
343 al., 2016, In review).

344 3.2. R_{CO} values from radiocarbon measurements

345 From the simultaneous CO and radiocarbon measurements, we calculated an R_{CO} of
346 13.4 ± 1.3 mmol CO/mol CO_2 with a correlation coefficient (r^2) of 0.7, and a median value of



347 11.2 mmol CO/mol CO₂. If we split the data seasonally, R_{CO} values of 12.5 ± 3.3 mmol
348 CO/mol CO₂ and 14.1 ± 4.0 mmol CO/mol CO₂ were obtained during winter and summer,
349 respectively. The slightly lower R_{CO} during winter is due to larger CO_{2ff} share during this
350 period from domestic heating. Our estimate is well within the range of values from previous
351 studies (10-15 mmol/mol) observed at other sites in Europe and North America (Gamnitzer et
352 al., 2006; Vogel et al., 2010; Turnbull et al., 2011). To test the sensitivity of this ratio to the
353 selection of background site, we additionally calculated R_{CO} using background values
354 estimated with the REBS method from the in-situ CO measurements at Beromünster instead
355 of Jungfraujoch. The value obtained in this way (12.7 ± 1.2, r² = 0.6) is only slightly lower
356 than the value obtained using Jungfraujoch as background site. Considering the persistent
357 decrease in CO emissions (Zellweger et al., 2009) in response to the European emission
358 legislation, our estimated R_{CO} is surprisingly high.

359 3.3. ΔCO/ΔCO₂ from continuous measurements

360 Figure 3 shows the seasonally resolved ΔCO to ΔCO₂ correlations derived from in-situ
361 measured CO and CO₂ enhancements over the background observed at Jungfraujoch, and we
362 have estimated a tracer ratio of 8.3 ± 0.1 mmol/mol (r² = 0.5) for the entire measurement
363 period. From measurements during winter, when the two species are most strongly correlated,
364 a ΔCO/ΔCO₂ ratio of 7.3 ± 0.1 mmol/mol (r² = 0.9) is obtained, while barely any correlation
365 is observed in summer and weak correlations (r² < 0.4) during spring and autumn. Recently,
366 Oney et al. (2016) reported a higher wintertime ratio of 8.3 mmol/mol for the same
367 combination of measurements at Beromünster and Jungfraujoch but for a different time
368 period. If we consider only winter 2013 as in their data, we obtain essentially the same value,
369 while much lower ratios of 6.5 mmol/mol and 6.4 mmol/mol were calculated for 2014 and
370 2015, respectively. The higher ratios in winter 2013 are likely related to the unusually cold
371 conditions and extended periods of air mass transport from Eastern Europe. Note that these



372 enhancement ratios also include emissions from non-fossil sources such as biofuels and
373 biomass burning in contrast to R_{CO} . The national inventory attributes about 15 % of total CO_2
374 emissions in 2014 to non-fossil fuel sources (FOEN, 2015b). If we correct for these sources
375 assuming a constant contribution throughout the year, the winter time $\Delta CO/\Delta CO_2$ ratio for the
376 three year data becomes 8.7 mmol/mol. This ratio is roughly consistent with the
377 anthropogenic CO to CO_2 emission ratio of 7.8 mmol/mol calculated from Switzerland's
378 greenhouse gas inventory report for 2013 (FOEN, 2015b, a). The slightly higher value points
379 towards an underestimation of the CO emissions by the inventory.

380 This wintertime $\Delta CO/\Delta CO_2$ ratio of 8.7 mmol/mol is still about 30 % lower than the
381 R_{CO} estimate for the same period (12.5 mmol/mol) shown as a black line in Fig. 3. This
382 suggests that despite the strong correlation between ΔCO and ΔCO_2 in winter the regional
383 CO_2 enhancements are not only caused by anthropogenic emissions but include a significant
384 biospheric CO_2 component. This also implies that the observed correlation is not only due to
385 spatially and temporally correlated sources but is caused to a large extent by meteorological
386 variability associated with more or less accumulation of trace gases in the boundary layer
387 irrespective of their origin. This interpretation is supported by the fact that a strong correlation
388 ($r^2 > 0.7$) was also observed between CO and CH_4 during winter at the same tower site (Satar
389 et al., 2016) despite their sources being vastly distinct. In Switzerland about 80 % of CH_4
390 emissions are from agriculture (mainly from ruminants) while more than 85 % of CO
391 emissions are from the transport sector and residential heating (FOEN, 2015a).

392 As a consequence, the true ratio of CO to anthropogenic CO_2 may be significantly
393 larger than the observed $\Delta CO/\Delta CO_2$ ratio of 8.7 mmol/mol, which in turn would imply that
394 the molar ratio of the Swiss emission inventory of 7.8 mmol/mol is too small.

395 **3.4. High resolution time series of CO_{2ff} and CO_{2bio}**



396 Figure 4 shows the hourly mean CO mixing ratios at Jungfraujoch and Beromünster
397 between 2013 and 2015. CO mixing ratios as high as 480 ppb were recorded at Beromünster
398 while generally lower CO values were recorded at the more remote site Jungfraujoch. A
399 pronounced seasonality in CO can be observed at Beromünster with higher values in winter
400 and lower values during summer due to stronger vertical mixing and chemical depletion of
401 CO by OH (Satar et al., 2016). The hourly mean CO_{2ff} time series calculated using these
402 continuous CO measurements and the seasonally resolved R_{CO} values derived using the
403 radiocarbon measurements are displayed in Fig. 4c. A seasonal trend in the calculated CO_{2ff} is
404 observed with frequent spikes of CO_{2ff} during winter while summer values show less
405 variability. We calculated a monthly mean amplitude (peak-to-trough) of 6.3 ppm with a
406 maximum in February and a minimum in July. During the measurement period, we have
407 observed CO_{2ff} mixing ratios ranging up to 27 ppm coinciding with cold periods and likely
408 from enhanced anthropogenic emissions due to heating. Instances of slightly negative CO_{2ff}
409 contributions, which occurred during less than 5 % of the time, were associated with negative
410 enhancements in CO (i.e. $\Delta\text{CO} < 0$). This could be simply due to an overestimation of
411 background values by the REBS function during these periods.

412 Figure 5a shows the hourly averaged residual CO_{2bio} values which exhibit a clear
413 seasonal cycle but also a considerable scatter in all seasons ranging from -13 ppm to +30
414 ppm. During winter, most values were close to zero or positive, implying a dominance of
415 respiration fluxes. In summer, conversely, pronounced negative and positive excursions were
416 observed mostly due to the diurnal cycle in net CO₂ fluxes, which are dominated by
417 photosynthetic uptake during daytime and respiration at night. Another factor contributing to
418 such variations may be the application of a constant emission ratio neglecting any diurnal
419 variability (Vogel et al., 2010).



420 It should also be noted that any non-fossil fuel CO₂ sources such as emissions from
421 biofuels would be incorporated into the CO_{2bio} term since CO_{2ff} in Eq. (1) represents the
422 fossil-fuel sources only, adding more variability to the data set. In order to reduce the
423 influence of these diurnal factors, we have looked into afternoon CO_{2bio} values (12:00 - 15:00
424 UTC), when the CO₂ mixing ratios along the tower are uniform (Satar et al., 2016) and R_{CO}
425 variability is minimal. Similar to the seasonal pattern in Fig. 5a, a clear seasonal cycle in
426 biospheric CO₂ can be observed (Fig. 5b) in agreement with biospheric exchange, but both
427 positive and negative extremes are less frequently observed (-12 ppm to +22 ppm).

428 The variation in CO_{2bio} during afternoon (12:00 – 15:00 UTC) was recently estimated
429 at this site to a range of -20 ppm to +20 ppm by combining observations and model
430 simulations for the year 2013 (Oney et al., 2016, In review). Our estimates are more positive
431 when compared to their study, due to the higher R_{CO} which results in lower CO_{2ff} and
432 correspondingly higher CO_{2bio} values.

433 Biospheric CO₂ shows a seasonally dependent diurnal variation as shown in Fig. 6.
434 During winter (Dec - Feb), the biospheric CO₂ component remains consistently positive (+2
435 to +5 ppm) throughout the day, implying net respiration fluxes. In summer, a clear feature
436 with increasing CO_{2bio} values during the night peaking between 07:00 and 08:00 UTC (i.e.
437 between 08:00 and 09:00 local time) can be observed. This buildup during the night can be
438 explained by CO₂ from respiration fluxes accumulating in the stable and shallow nocturnal
439 boundary layer. Then, after sunrise, the early morning CO_{2bio} peak starts to gradually decrease
440 due to a combination of onset of photosynthesis and enhanced vertical mixing due to the
441 growth of the boundary layer. At Beromünster, a decrease in CO₂ mixing ratios from both
442 processes is visible more or less at the same time at the 212.5 m height level, while at the
443 lowest inlet level (12.5 m) the photosynthetic uptake signal is observed about an hour earlier
444 (Satar et al., 2016). Between 12:00 and 15:00 UTC, when the daytime convective boundary



445 layer is fully established, the biospheric CO_2 continues to become more negative implying net
446 photosynthetic uptake, which eventually stabilizes for 3 - 5 hours until nighttime $\text{CO}_{2\text{bio}}$
447 accumulation starts.

448 **4. Conclusions**

449 From continuous measurements of CO and CO_2 and bi-weekly radiocarbon samples at
450 the Beromünster tall tower, we have estimated a ΔCO to $\Delta\text{CO}_{2\text{ff}}$ ratio (R_{CO}) which was
451 subsequently used to construct a 3-years long high-resolution $\text{CO}_{2\text{ff}}$ time series. We have
452 corrected the ratio for an offset of about 16 % caused by ^{14}C emissions from nearby NPPs.
453 This bias was calculated by comparing the simulated mean enhancement in $\Delta^{14}\text{C}$ (1.6 ‰) due
454 to NPPs with the measured mean depletion in $\Delta^{14}\text{C}$ due to fossil fuel CO_2 (9.9 ‰). The
455 radiocarbon-based R_{CO} derived in this study during winter is significantly higher than the
456 $\text{CO}:\text{CO}_2$ enhancement ratios estimated from continuous CO and CO_2 measurements during
457 the same period, suggesting a significant biospheric contribution to regional CO_2
458 enhancements during this period.

459 The obtained $\text{CO}_{2\text{ff}}$ time series shows a clear seasonality with frequent spikes during
460 winter associated with enhanced anthropogenic emissions and weak vertical mixing while
461 summer values are mostly stable.

462 By subtracting the estimated $\text{CO}_{2\text{ff}}$ and $\text{CO}_{2\text{bg}}$ from $\text{CO}_{2\text{meas}}$, we have also calculated
463 the biospheric CO_2 component, which ranges between -15 ppm and +30 ppm. Considering
464 only afternoon data (12:00 – 15:00 UTC) when the convective boundary layer is fully
465 established, $\text{CO}_{2\text{bio}}$ showed its minimum in summer coinciding with net photosynthetic uptake
466 but still with frequent positive excursions possibly due to biomass burning or enhanced
467 soil/plants exhalation. During winter, $\text{CO}_{2\text{bio}}$ becomes nearly zero or positive, implying
468 respiration fluxes.



469 A pronounced diurnal variation in $\text{CO}_{2\text{bio}}$ was observed during summer modulated by
470 vertical mixing and biospheric exchange while this variation disappears during winter.
471 However, the variation in $\text{CO}_{2\text{bio}}$ may also be influenced by the uncertainty of the $\text{CO}_{2\text{ff}}$
472 estimate especially due to applying a constant emission ratio while calculating $\text{CO}_{2\text{ff}}$. Hence,
473 it will be important in the future to include seasonally and diurnally resolved R_{CO} values from
474 high-frequency radiocarbon measurements to better estimate $\text{CO}_{2\text{ff}}$. Additionally, including
475 independent tracers such as Atmospheric Potential Oxygen (APO) estimates based on
476 concurrent CO_2 and O_2 measurements will be very useful to validate fossil-fuel emission
477 estimates from the radiocarbon method. This technique is also advantageous as the fossil fuel
478 CO_2 estimate is unaltered by contribution from NPPs as well as it accounts for the
479 contribution from biofuels.

480

481 **Acknowledgements**

482 This project was funded by the Swiss National Science Foundation through the Sinergia
483 project CarboCount CH (CRSII2 136273). We are also grateful to the ICOS-Switzerland and
484 the International Foundation High Alpine Research Stations Jungfrauoch and Gornergrat.
485 The LARA laboratory would like to thank René Fischer for the production of large CO_2
486 amounts by combustion of the NIST standard oxalic acid II, and Dejan Husrefovic for the
487 evaluation of the sample transfer line. Finally, we would like to thank Heather Graven and
488 Nicolas Gruber for helpful input regarding radiocarbon emissions from NPPs and the Swiss
489 Federal Nuclear Safety Inspectorate (ENSI) and the Berner Kraftwerke (BKW) for fruitful
490 discussions and providing radiocarbon emission data.

491

492

493



494 List of Tables and Figures

495 Table 1. Ratios (R_{CO}) determined using radiocarbon measurements after correcting for
496 influence from NPPs and applying model II regression, and ratios derived from continuous
497 CO and CO₂ measurements by the CRDS analyzer as enhancements ($\Delta CO:\Delta CO_2$) using
498 Jungfraujoch background measurements. R_{CO} values are given in mmol/mol with standard
499 uncertainties of the slope and r^2 values in brackets and n represents the number of samples for
500 the radiocarbon method. Note that according to the Swiss emission inventory report for
501 greenhouse gas emissions in 2013, the annual anthropogenic CO/CO₂ emission ratio for the
502 national estimate is 7.8 mmol/mol.

	R_{CO} ($\Delta CO:\Delta CO_{2ff}$) (radiocarbon)	Number of samples (n)	$\Delta CO:\Delta CO_2$ (CRDS)
Winter (Dec-Feb)	12.5 ± 3.3 (0.6)	8	7.3 (0.9)
Summer (Jun-Aug)	14.1 ± 4.0 (0.3)	14	13.4 (0.02)
All data	13.4 ± 1.3 (0.6)	45	8.3 (0.5)

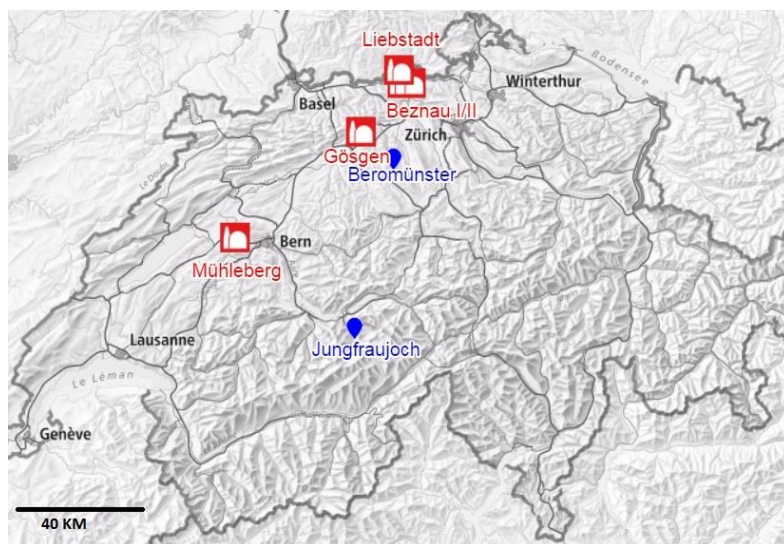
503

504

505

506

507



508

509 Figure 1. The geographical map of Beromünster and Jungfrauoch measurement sites (blue) as
510 well as the five NPPs in Switzerland (red).

511

512

513

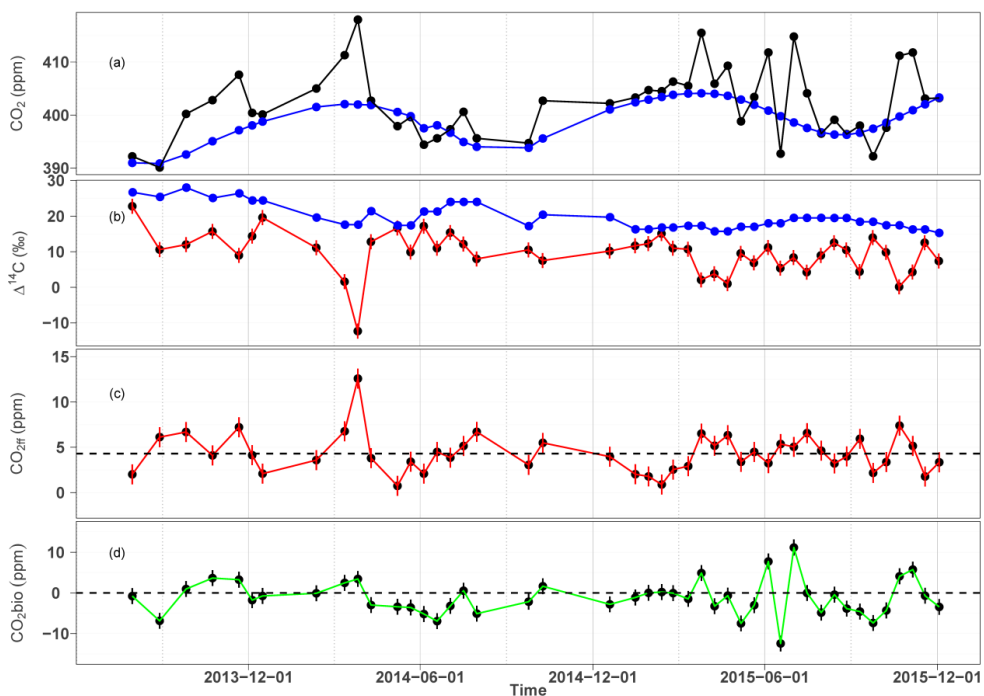
514

515

516

517

518

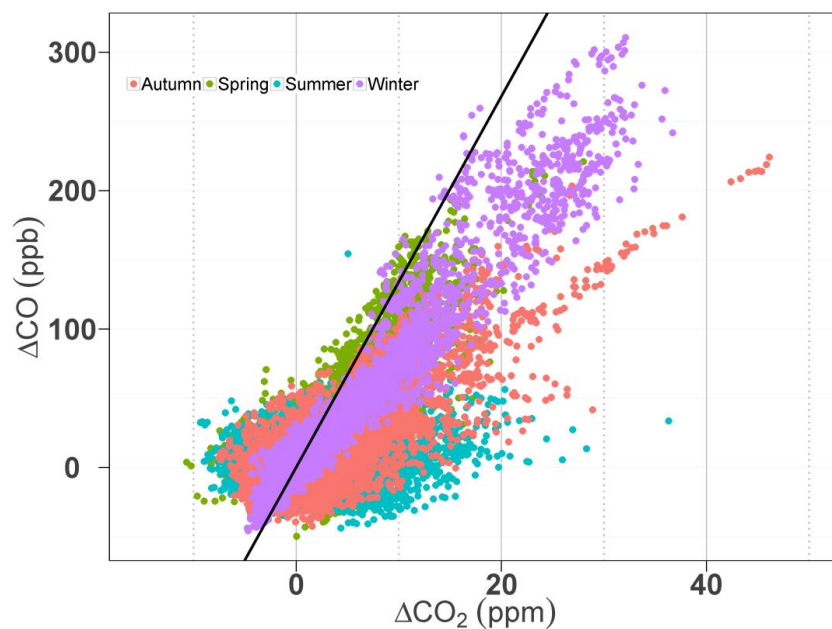


519

520 Figure 2. CO₂ mixing ratios (hourly averages) at Beromünster (black) from the sample inlet at
521 212.5 m and from background measurements at Jungfraujoch (blue) filtered using the REBS
522 function for periods when ¹⁴C sampling was conducted (a), Δ¹⁴C determined from the bi-
523 weekly point samplings at the site (red) and from 14-days integrated samplings at
524 Jungfraujoch (blue) (b), CO_{2ff} determined during this period applying Eq. (4) with a mean
525 CO_{2ff} value of 4.3 ppm (dashed line) (c), and the biospheric CO₂ determined by simple
526 subtraction of CO_{2bg} and CO_{2ff} from the CO_{2meas} (d). Error bars in (b) and (c) indicate the
527 mean uncertainty in Δ¹⁴C measurement (± 2.1 ‰) and calculated CO_{2ff} (± 1.1 ppm), averaged
528 for the triplicate samples while error bar in (d) is obtained from error propagation of the
529 components in (a), (b) and (c). CO₂ mixing ratios in the top panel are only shown from times
530 matching the radiocarbon sampling at Beromünster tower.

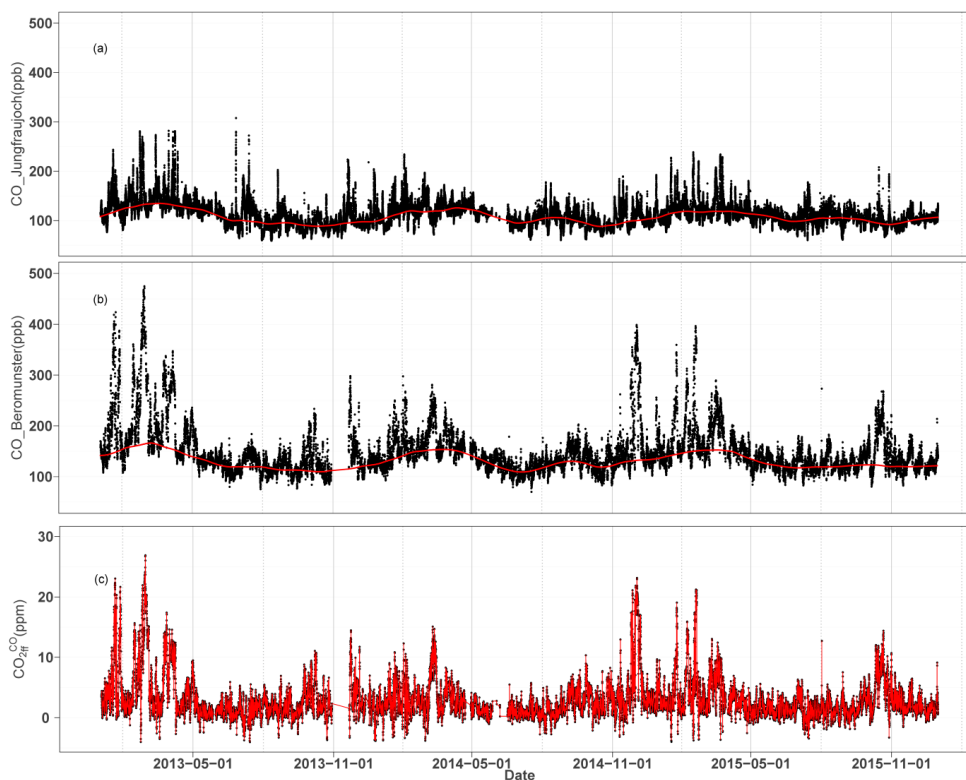
531

532



533

534 Figure 3. The correlation between enhancements in CO and CO₂ at Beromünster over
535 Jungfraujoch background for the different seasons. The black solid line shows the wintertime
536 R_{CO} derived from radiocarbon measurements.



537

538 Figure 4. Time series of hourly mean CO mixing ratios measured at Jungfraujoch (a) and
539 Beromünster (b) sites with the red curve showing the estimated background values using the
540 REBS method with 60 days window. Panel (c) shows the hourly mean CO_{2ff} time series
541 calculated using the emission ratios determined from radiocarbon measurements, and the CO
542 enhancements at Beromünster over the Jungfraujoch background based on Eq. (6).

543

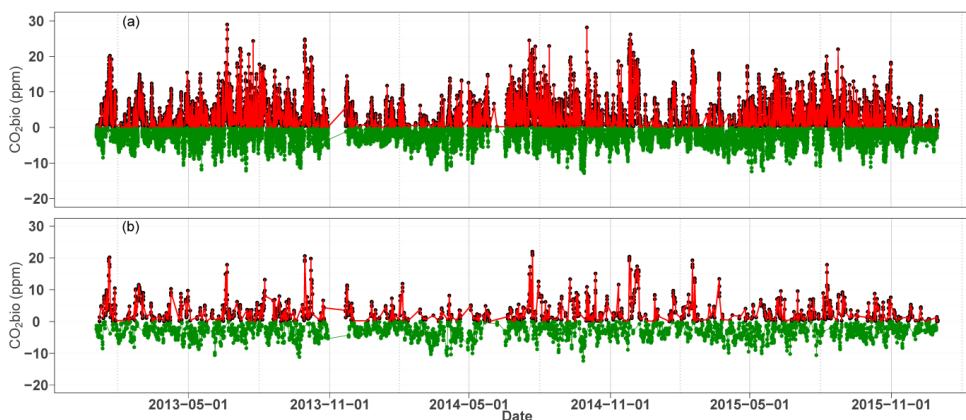
544

545

546

547

548

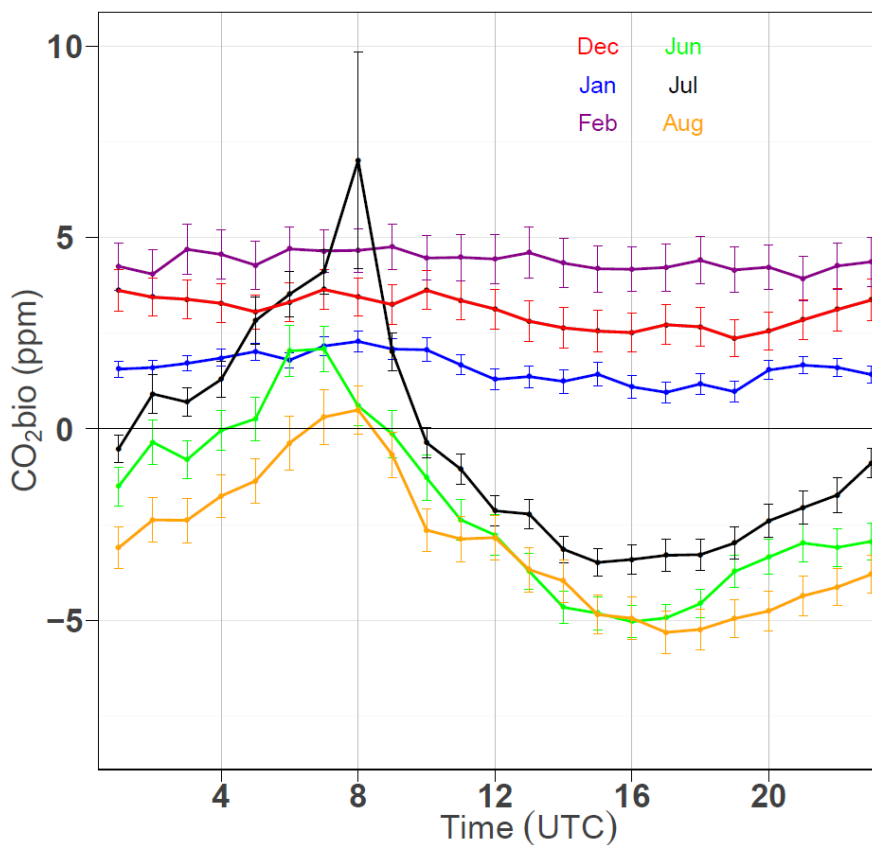


549

550 Figure 5. Time series (hourly resolution) of the biospheric CO_2 derived as a residual of the
551 difference between the total CO_2 , $\text{CO}_{2\text{bg}}$ and $\text{CO}_{2\text{ff}}$ for all data (a), and only afternoon data
552 from 12:00-15:00 UTC (b). The green lines show negative $\text{CO}_{2\text{bio}}$ implying uptake while red
553 ones represent positive $\text{CO}_{2\text{bio}}$. The average uncertainty of $\text{CO}_{2\text{bio}}$ amounts ± 1.3 ppm
554 calculated from error propagation.

555

556



557

558 Figure 6. Hourly variations of monthly averaged biospheric CO₂ during summer (Jun – Aug)
559 and winter (Dec – Feb). While winter values dominated by respiration are constant throughout
560 a day, summer values show a significant diurnal variation induced by photosynthesis and
561 vertical mixing. The error bars are the standard deviations of the hourly averaged CO_{2bio}
562 values for each month.

563

564

565

566

567



568 **References**

- 569 Ballantyne, A. P., Andres, R., Houghton, R., Stocker, B. D., Wanninkhof, R., Anderegg, W., Cooper, L.
570 A., DeGrandpre, M., Tans, P. P., Miller, J. B., Alden, C., and White, J. W. C.: Audit of the global carbon
571 budget: estimate errors and their impact on uptake uncertainty, *Biogeosciences*, 12, 2565-2584,
572 10.5194/bg-12-2565-2015, 2015.
- 573 Basu, S., Miller, J. B., and Lehman, S.: Separation of biospheric and fossil fuel fluxes of CO₂ by
574 atmospheric inversion of CO₂ and ¹⁴CO₂ measurements: Observation System Simulations, *Atmos*
575 *Chem Phys*, 16, 5665-5683, 10.5194/acp-16-5665-2016, 2016.
- 576 Berhanu, T. A., Satar, E., Schanda, R., Nyfeler, P., Moret, H., Brunner, D., Oney, B., and Leuenberger,
577 M.: Measurements of greenhouse gases at Beromünster tall tower station in Switzerland, *Atmos.*
578 *Meas. Tech.*, 9, 10.5194/amt-9-2603-2016, 2016.
- 579 Ciais, P., Paris, J. D., Marland, G., Peylin, P., Piao, S. L., Levin, I., Pregger, T., Scholz, Y., Friedrich, R.,
580 Rivier, L., Houwelling, S., Schulze, E. D., and Team, C. S.: The European carbon balance. Part 1: fossil
581 fuel emissions, *Glob Change Biol*, 16, 1395-1408, DOI 10.1111/j.1365-2486.2009.02098.x, 2010.
- 582 Currie, L. A.: The remarkable metrological history of radiocarbon dating [II], *J Res Natl Inst Stan*, 109,
583 185-217, 10.6028/jres.109.013, 2004.
- 584 FOEN: Switzerland's Informative Inventory Report 2015, Swiss Federal Office for the Environment
585 2015a.
- 586 FOEN: Switzerland's Greenhouse Gas Inventory 1990-2013, Swiss Federal Office for the Environment
587 2015b.
- 588 Friedlingstein, P., Houghton, R. A., Marland, G., Hackler, J., Boden, T. A., Conway, T. J., Canadell, J. G.,
589 Raupach, M. R., Ciais, P., and Le Quere, C.: Update on CO₂ emissions, *Nat Geosci*, 3, 811-812, Doi
590 10.1038/Ngeo1022, 2010.
- 591 Gamnitzer, U., Karstens, U., Kromer, B., Neubert, R. E. M., Meijer, H. A. J., Schroeder, H., and Levin, I.:
592 Carbon monoxide: A quantitative tracer for fossil fuel CO₂?, *J Geophys Res-Atmos*, 111, Artn D22302



- 593 Doi 10.1029/2005jd006966, 2006.
- 594 Graven, H. D., and Gruber, N.: Continental-scale enrichment of atmospheric $^{14}\text{CO}_2$ from the nuclear
595 power industry: potential impact on the estimation of fossil fuel-derived CO_2 , Atmos. Chem. Phys.,
596 11, 12339-12349, 10.5194/acp-11-12339-2011, 2011.
- 597 Hammer, S., Friedrich, R., Kromer, B., Cherkinsky, A., Lehman, S. J., Meijer, H. A. J., Nakamura, T.,
598 Palonen, V., Reimer, R. W., Smith, A. M., Southon, J. R., Szidat, S., Turnbull, J., and Uchida, M.:
599 Compatibility of Atmospheric $^{14}\text{CO}_2$ Measurements: Comparing the Heidelberg Low-Level Counting
600 Facility to International Accelerator Mass Spectrometry (AMS) Laboratories, Radiocarbon, 1-9,
601 10.1017/RDC.2016.62, 2016.
- 602 Heimann, M., and Reichstein, M.: Terrestrial ecosystem carbon dynamics and climate feedbacks,
603 Nature, 451, 289-292, 10.1038/nature06591, 2008.
- 604 Henne, S., Brunner, D., Oney, B., Leuenberger, M., Eugster, W., Bamberger, I., Meinhardt, F.,
605 Steinbacher, M., and Emmenegger, L.: Validation of the Swiss methane emission inventory by
606 atmospheric observations and inverse modelling, Atmos Chem Phys, 16, 3683-3710, 2016.
- 607 Le Quéré, C., Andrew, R. M., Canadell, J. G., Sitch, S., Korsbakken, J. I., Peters, G. P., Manning, A. C.,
608 Boden, T. A., Tans, P. P., Houghton, R. A., Keeling, R. F., Alin, S., Andrews, O. D., Anthoni, P., Barbero,
609 L., Bopp, L., Chevallier, F., Chini, L. P., Ciais, P., Currie, K., Delire, C., Doney, S. C., Friedlingstein, P.,
610 Gkritzalis, T., Harris, I., Hauck, J., Haverd, V., Hoppema, M., Klein Goldewijk, K., Jain, A. K., Kato, E.,
611 Körtzinger, A., Landschützer, P., Lefèvre, N., Lenton, A., Lienert, S., Lombardozi, D., Melton, J. R.,
612 Metzl, N., Millero, F., Monteiro, P. M. S., Munro, D. R., Nabel, J. E. M. S., Nakaoka, S. I., O'Brien, K.,
613 Olsen, A., Omar, A. M., Ono, T., Pierrot, D., Poulter, B., Rödenbeck, C., Salisbury, J., Schuster, U.,
614 Schwinger, J., Séférian, R., Skjelvan, I., Stocker, B. D., Sutton, A. J., Takahashi, T., Tian, H., Tilbrook, B.,
615 van der Laan-Luijkx, I. T., van der Werf, G. R., Viovy, N., Walker, A. P., Wiltshire, A. J., and Zaehle, S.:
616 Global Carbon Budget 2016, Earth Syst. Sci. Data, 8, 605-649, 10.5194/essd-8-605-2016, 2016.



- 617 Leuenberger, M. C., Eyer, M., Nyfeler, P., Stauffer, B., and Stocker, T. F.: High-resolution¹³C
618 measurements on ancient air extracted from less than 10 cm(3) of ice, *Tellus B*, 55, 138-144, DOI
619 10.1034/j.1600-0889.2003.01463.x, 2003.
- 620 Levin, I., Kromer, B., Schmidt, M., and Sartorius, H.: A novel approach for independent budgeting of
621 fossil fuel CO₂ over Europe by ¹⁴CO₂ observations, *Geophys Res Lett*, 30, Doi 10.1029/2003gl018477,
622 2003.
- 623 Levin, I., and Karstens, U.: Inferring high-resolution fossil fuel CO₂ records at continental sites from
624 combined ¹⁴CO₂ and CO observations, *Tellus B*, 59, 245-250, DOI 10.1111/j.1600-0889.2006.00244.x,
625 2007.
- 626 Levin, I., Naegler, T., Kromer, B., Diehl, M., Francey, R. J., Gomez-Pelaez, A. J., Steele, L. P.,
627 Wagenbach, D., Weller, R., and Worthy, D. E.: Observations and modelling of the global distribution
628 and long-term trend of atmospheric (CO₂)-C-14 (vol 62, pg 26, 2010), *Tellus B*, 62, 207-207,
629 10.1111/j.1600-0889.2010.00456.x, 2010.
- 630 Levin, I., Kromer, B., and Hammer, S.: Atmospheric Delta ¹⁴CO₂ trend in Western European
631 background air from 2000 to 2012, *Tellus B*, 65, DOI 10.3402/tellusb.v65i0.20092, 2013.
- 632 Loosli, H. H., and Oeschger, H.: C-14 in the Environment of Swiss Nuclear Installations, *Radiocarbon*,
633 31, 747-753, 1989.
- 634 Lopez, M., Schmidt, M., Delmotte, M., Colomb, A., Gros, V., Janssen, C., Lehman, S. J., Mondelain, D.,
635 Perrussel, O., Ramonet, M., Xueref-Remy, I., and Bousquet, P.: CO, NO_x and ¹³CO₂ as tracers for fossil
636 fuel CO₂: results from a pilot study in Paris during winter 2010, *Atmos Chem Phys*, 13, 7343-7358, DOI
637 10.5194/acp-13-7343-2013, 2013.
- 638 Marland, G.: Uncertainties in accounting for CO₂ from fossil fuels, *J Ind Ecol*, 12, 136-139, DOI
639 10.1111/j.1530-9290.2008.00014.x, 2008.
- 640 Marland, G., Hamal, K., and Jonas, M.: How Uncertain Are Estimates of CO₂ Emissions ?, *J Ind Ecol*,
641 13, 4-7, DOI 10.1111/j.1530-9290.2009.00108.x, 2009.



- 642 Nemec, M., Wacker, L., and Gaggeler, H.: Optimization of the Graphitization Process at Age-1,
643 Radiocarbon, 52, 1380-1393, 2010.
- 644 Oney, B., Henne, S., Gruber, N., Leuenberger, M., Bamberger, I., Eugster, W., and Brunner, D.: The
645 CarboCount CH sites: characterization of a dense greenhouse gas observation network, Atmos.
646 Chem. Phys., 15, 11147-11164, 10.5194/acp-15-11147-2015, 2015.
- 647 Oney, B., Gruber, N., Henne, S., Leuenberger, M., and Brunner, D.: A CO-based method to determine
648 the regional biospheric signal in atmospheric CO₂, in, Tellus, 2016, In review.
- 649 Peylin, P., Houweling, S., Krol, M. C., Karstens, U., Rödenbeck, C., Geels, C., Vermeulen, A., Badawy,
650 B., Aulagnier, C., Pregger, T., Delage, F., Pieterse, G., Ciais, P., and Heimann, M.: Importance of fossil
651 fuel emission uncertainties over Europe for CO₂ modeling: model intercomparison, Atmos. Chem.
652 Phys., 11, 6607-6622, 10.5194/acp-11-6607-2011, 2011.
- 653 Ruckstuhl, A. F., Henne, S., Reimann, S., Steinbacher, M., Vollmer, M. K., O'Doherty, S., Buchmann, B.,
654 and Hueglin, C.: Robust extraction of baseline signal of atmospheric trace species using local
655 regression, Atmos Meas Tech, 5, 2613-2624, DOI 10.5194/amt-5-2613-2012, 2012.
- 656 Satar, E., Berhanu, T. A., Brunner, D., Henne, S., and Leuenberger, M.: Continuous CO₂/CH₄/CO
657 measurements (2012-2014) at Beromünster tall tower station in Switzerland, Biogeosciences
658 Discuss., 13, 2623-2635, 10.5194/bg-13-2623-2016, 2016.
- 659 Schibig, M. F., Mahieu, E., Henne, S., Lejeune, B., and Leuenberger, M. C.: Intercomparison of in situ
660 NDIR and column FTIR measurements of CO₂ at Jungfrauoch, Atmos Chem Phys, 16, 9935-9949,
661 10.5194/acp-16-9935-2016, 2016.
- 662 Szidat, S., Salazar, G. A., Vogel, E., Battaglia, M., Wacker, L., Synal, H. A., and Turler, A.: ¹⁴C Analysis
663 and Sample Preparation at the New Bern Laboratory for the Analysis of Radiocarbon with AMS
664 (LARA), Radiocarbon, 56, 561-566, 10.2458/56.17457, 2014.



- 665 Tolk, L. F., Meesters, A. G. C. A., Dolman, A. J., and Peters, W.: Modelling representation errors of
666 atmospheric CO₂ mixing ratios at a regional scale, Atmos. Chem. Phys., 8, 6587-6596, 10.5194/acp-8-
667 6587-2008, 2008.
- 668 Turnbull, J., Rayner, P., Miller, J., Naegler, T., Ciais, P., and Cozic, A.: On the use of ¹⁴CO₂ as a tracer for
669 fossil fuel CO₂: Quantifying uncertainties using an atmospheric transport model, J Geophys Res-
670 Atmos, 114, 10.1029/2009jd012308, 2009.
- 671 Turnbull, J. C., Miller, J. B., Lehman, S. J., Tans, P. P., Sparks, R. J., and Southon, J.: Comparison of
672 ¹⁴CO₂, CO, and SF₆ as tracers for recently added fossil fuel CO₂ in the atmosphere and implications for
673 biological CO₂ exchange, Geophys Res Lett, 33, Doi 10.1029/2005gl024213, 2006.
- 674 Turnbull, J. C., Karion, A., Fischer, M. L., Faloona, I., Guilderson, T., Lehman, S. J., Miller, B. R., Miller,
675 J. B., Montzka, S., Sherwood, T., Saripalli, S., Sweeney, C., and Tans, P. P.: Assessment of fossil fuel
676 carbon dioxide and other anthropogenic trace gas emissions from airborne measurements over
677 Sacramento, California in spring 2009, Atmos Chem Phys, 11, 705-721, 10.5194/acp-11-705-2011,
678 2011.
- 679 Turnbull, J. C., Keller, E. D., Baisden, T., Brailsford, G., Bromley, T., Norris, M., and Zondervan, A.:
680 Atmospheric measurement of point source fossil CO₂ emissions, Atmos Chem Phys, 14, 5001-5014,
681 DOI 10.5194/acp-14-5001-2014, 2014.
- 682 Turnbull, J. C., Sweeney, C., Karion, A., Newberger, T., Lehman, S. J., Tans, P. P., Davis, K. J., Lauvaux,
683 T., Miles, N. L., Richardson, S. J., Cambaliza, M. O., Shepson, P. B., Gurney, K., Patarasuk, R., and
684 Razlivanov, I.: Toward quantification and source sector identification of fossil fuel CO₂ emissions from
685 an urban area: Results from the INFLUX experiment, J Geophys Res-Atmos, 120, 292-312,
686 10.1002/2014JD022555, 2015.
- 687 Vogel, F. R., Hammer, S., Steinhof, A., Kromer, B., and Levin, I.: Implication of weekly and diurnal ¹⁴C
688 calibration on hourly estimates of CO-based fossil fuel CO₂ at a moderately polluted site in
689 southwestern Germany, Tellus B, 62, 512-520, DOI 10.1111/j.1600-0889.2010.00477.x, 2010.



- 690 Wacker, L., Christl, M., and Synal, H. A.: Bats: A new tool for AMS data reduction, Nucl Instrum Meth
691 B, 268, 976-979, 10.1016/j.nimb.2009.10.078, 2010.
- 692 Yim, M. S., and Caron, F.: Life cycle and management of carbon-14 from nuclear power generation,
693 Prog Nucl Energ, 48, 2-36, 10.1016/j.pnucene.2005.04.002, 2006.
- 694 Zellweger, C., Hugglin, C., Klausen, J., Steinbacher, M., Vollmer, M., and Buchmann, B.: Inter-
695 comparison of four different carbon monoxide measurement techniques and evaluation of the long-
696 term carbon monoxide time series of Jungfraujoch, Atmos Chem Phys, 9, 3491-3503, 2009.
- 697 Zellweger, C., Steinbacher, M., and Buchmann, B.: Evaluation of new laser spectrometer techniques
698 for in-situ carbon monoxide measurements, Atmos Meas Tech, 5, 2555-2567, 10.5194/amt-5-2555-
699 2012, 2012.
- 700 Zondervan, A., and Meijer, H. A. J.: Isotopic characterisation of CO₂ sources during regional pollution
701 events using isotopic and radiocarbon analysis, Tellus B, 48, 601-612, DOI 10.1034/j.1600-
702 0889.1996.00013.x, 1996.
- 703
- 704
- 705
- 706